Energy harvesting and propulsion of pitching airfoils with passive heave and deformation

Ramon Fernandez-Feria* and Javier Alaminos-Quesada†
Fluid Mechanics Group, University of Málaga, Dr Ortiz Ramos s/n, 29071 Málaga, Spain

A general formulation for the fluid-structure interaction of an airfoil undergoing prescribed pitching and passive heave and deformation about an arbitrary axis is given in the linearized potential flow limit. The resulting three algebraic equations provide the heave and deformation amplitudes linearly from two of the equations, and the torque that generates the pitching motion, and hence the input power, from the third. Both, the energy harvesting and the propulsion problems are analyzed. In the first case, energy is harvested at the pivot point through dampers, so that the efficiency is obtained once the heaving motion and the input power are computed. In the second problem, the prescribed pitch and the computed heave and deformation yield the thrust, and the propulsive efficiency with the obtained input power. The present analytical results allow for a general survey of these two physical problems as the multiple governing parameters are varied. It is generally found that the best performance is achieved around the first natural frequency, which is obtained here from a simple algebraic expression. The formulation is validated with previous experimental and numerical results. The effect of flexibility maximizing the energy harvesting efficiency is particularly analyzed.

I. Nomenclature

a	=	nondimensional pivot point location	k_α	=	nondimensional torsional spring constant
b_h	=	nondimensional linear damper constant	k_r	=	nondimensional natural frequency
b_α	=	nondimensional torsional damper constant	k_{r0}	=	nondimensional natural frequency in vacuum
c	=	chord length	m	=	nondimensional mass of the foil
C_F	=	flexural coefficient	R	=	mass ratio, $R = \rho_s \varepsilon/(\rho c)$
C_L	=	lift coefficient	S	=	stiffness ratio, $S = E\varepsilon^3/(\rho U^2 c^3)$
C_{L_o}	=	output lift coefficient	U	=	flow speed
C_M	=	moment coefficient	x	=	nondimensional streamwise coordinate
C_{M_i}	=	input torque coefficient	x_0	=	nondimensional center of mass
C_{M_o}	=	output moment coefficient	z	=	nondimensional coordinate normal to the stream
C_{P_i}	=	input power coefficient	$z_s(x,t)$	=	nondimensional displacement of the foil
C_{Po}	=	output power coefficient	$\alpha(t)$	=	pitch angle

*Professor, Fluid Mechanics Dept.; ramon.fernandez@uma.es
†Post-Doctoral Researcher, Fluid Mechanics Dept.; jalaminos@uma.es

C_T	=	thrust coefficient	α_0	=	pitch amplitude
$d(t)$	=	nondimensional chordwise flexural deflection	ε	=	foil's thickness
d_m	=	nondimensional flexural deflection amplitude	η_e	=	energy harvesting efficiency
E	=	elastic modulus	η_p	=	propulsive efficiency
$h(t)$	=	nondimensional heaving motion	ρ	=	fluid density
h_0	=	nondimensional heaving amplitud	ρ_s	=	foil's density
I_a	=	nondimensional moment of inertia	ϕ	=	phase shift heave / pitch
k	=	reduced frequency, $k = \omega c/(2U)$	ψ	=	phase shift flexural deflection / pitch
k_h	=	nondimensional linear spring constant	ω	=	frequency

II. Introduction

The aero-hydro-dynamics of heaving and pitching foils have been investigated over several decades to understand animal swimming and flapping flight, as well as to find out configurations with optimal thrust production to use them as efficient bio-inspired propellers [1–3]. Both, thrust and propulsion efficiency can be greatly enhanced by taking advantage of the chordwise, passive flexibility of the foil over certain ranges of the structural and kinematic parameters [4–7]. Passive heave also produces much greater propulsive efficiency and reduces the minimal frequency for thrust production compared to a pitching-only motion of the foil, allowing simpler one-actuator devices to compete with more complex two-actuator devices for prescribed pitching and heaving motions. Murray and Howle [8] and Mackowski and Williamson [9] analyzed these semi-passive rigid-foils propulsors with prescribed pitch and passive heave. Some of their numerical [8] and experimental [9] results are compared with the present ones in §V.A.

In addition to propulsion purposes, oscillating foils have been widely investigated as energy harvesting devices to extract energy from natural currents and wind [10–16]. In particular, semi-passive flapping-foil turbines with forced pitching oscillations and passive heaving motion have shown some potential advantage in terms of energy harvesting efficiency [17–20], which may be more promising than fully-activated and fully-passive models [21]. Thus, Zhu and Peng [17] considered numerically the fluid-structure interaction of these semi-passive systems for energy harvesting with a pitching rigid foil at low Reynolds numbers (about 1000), neglecting the inertia of the foil, an effect that was later considered by Deng et al. [19], also numerically at about the same Reynolds number. Liu et al. [18] and Ma et al. [21] analyzed the problem numerically at much higher Reynolds numbers using different turbulence models. In fact, Ma et al. [21], who considered a wider range of the structural parameters, found energy harvesting efficiencies for rigid foils above 40%, greater than in previous similar studies. The semi-passive problem for a rigid foil was also studied experimentally by Su and Breuer [20] at Reynolds 10^4, covering a wide range of structural parameters and considering also nonsinusoidal pitch profiles. Some of their experimental data are compared in §V.B with the present results for a rigid foil.

The combined effect of passive heaving motion and chordwise flexibility in both problems (propulsion and energy harvesting) has been less explored. Although Liu et al. [18] also considered flexible foils in their numerical study

of these semi-passive systems for energy harvesting, finding a substantial increase of the efficiency in relation to the rigid foil counterpart, they used several types of prescribed wing deformations, and therefore without considering the fluid-structure interaction (FSI). Here we analyze the passive heave and deformation of the flexible pitching foil jointly from the standpoint of the FSI. In particular, it is proposed in the present work a general theory that yields analytical solutions for the energy harvesting and the propulsion performance of a flapping-foil device of this kind in the limit of small amplitude of the flapping and deformation motions for sufficiently high Reynolds numbers, so that the Euler-Bernoulli beam equation for the FSI combined with the linear, two-dimensional potential flow theory can be used. Apart from this limitation, the problem is formulated in the most general terms: for any pivot axis location and arbitrary mass distribution of the airfoil, so that any distance between the pivot point and the centre of mass is allowed, for any stiffness of the foil, and for any spring constant and actuating frequency. Use is made of general results from the vortical impulse theory recently derived for the thrust, lift, and moment on a airfoil undergoing any heaving and pitching motions superimposed to small flexural deformations [22], coupled with the structural dynamics of the foil governed by the Euler-Bernoulli beam equation [23, 24]. The limitation to small deflection amplitude, modeled by a quartic polynomial, restricts the theory to just capturing the first natural frequency of the fluid-airfoil system, but it is known that the maximum thrust is always obtained when the flexible foil is actuated with this first natural frequency [25]. Although previous linear theories, but without considering passive heaving, capture all the resonant modes of the system [26, 27], here the problem is greatly simplified to just solving a system of three algebraic equations, covering also the similar energy harvesting problem by selecting appropriate ranges of some of the nondimensional parameters. These analytical solutions are obtained with the present formulation because the simplifications in the FSI and because the afore-mentioned closed expressions derived from the vortex impulse theory for the fluid forces and torques. The frequency of the first resonant mode is obtained from a single algebraic expression containing all the nondimensional governing parameters, reproducing exactly results in the limit when the FSI is neglected well known in the literature. To validate the present theory, we compare with previous experimental and numerical results for pitching rigid foils with passive heave, showing an excellent agreement. It is found that flexibility is more relevant in the present flapping configuration for the efficiency of the energy harvesting devices than for the propulsion efficiency. In most cases, the best performance is connected to the resonant frequency, as previously obtained for similar flapping-foil systems [25, 27–31].

This work is an extension of Ref. [24], where the propulsion and energy harvesting performances of a flexible thin airfoil is analyzed when the heaving motion is prescribed and the pitching and deformation motions are induced by the FSI, instead of the present forced pitching motion with passive heave and deformation. Although it obviously shares some common elements, most of them given in the appendices, the algebraic equations governing the passive heave and deformation are different, and the results for the energy harvesting and the propulsive efficiencies are quite different indeed, as described in the following sections.

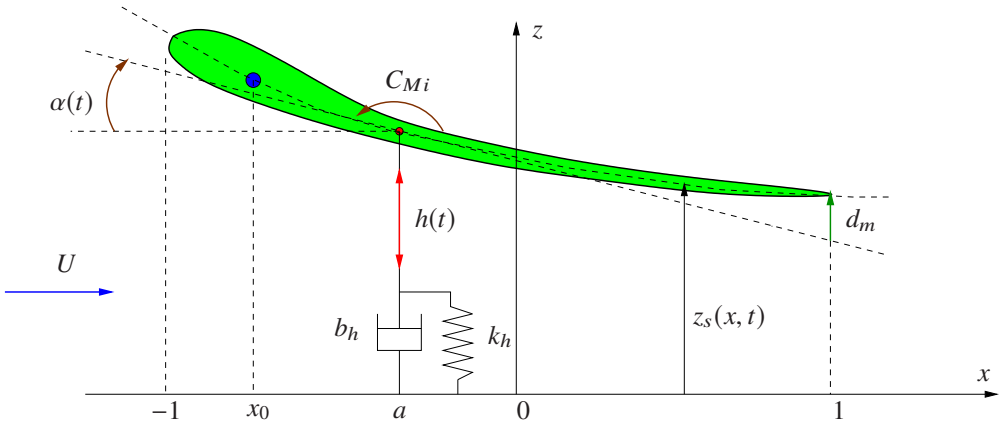

Fig. 1 Schematic of the semi-passive foil motion (all quantities are dimensionless, except the velocity U).

III. Formulation of the problem

Figure 1 shows a sketch of the semi-passive system consisting of a two-dimensional (2D) foil in an incompressible and inviscid flow with constant free-stream velocity U along the axis x. The foil undergoes a forced pitching motion with prescribed amplitude α_0 and frequency ω, generated by a controller that imparts an input torque (per unit span) M_i to the foil at the pivot point a, and which will be obtained below as part of the solution. We use dimensionless variables scaled with the speed U and the half-chord length $c/2$ (so that time t is nondimensionalized with $c/2U$). The pitching motion can be written as

$$\alpha(t) = \Re\left[\alpha_0 e^{ikt}\right], \quad k = \frac{\omega c}{2U}, \tag{1}$$

where $\Re$ means real part and k is the reduced frequency. The dimensionless input torque is $C_{M_i} = M_i/(\rho U^2 c^2/2)$, with ρ the fluid density.

The airfoil is allowed to undergo a superimposed passive heaving motion $h(t)$ along the axis z through the pivot point $x = a$, where the foil is elastically supported with a linear spring of nondimensional constant k_h. Additionally, it may also be connected to a linear damper of dimensionless constant b_h when the system is used as a device to extract energy from the current, with the generator simplified as a damper. In terms of these constants, the (dimensionless) output force C_{L_o} along the z-axis applied at $x = a$ is given by

$$C_{L_o} = \frac{L_o}{\frac{1}{2}\rho U^2 c} = k_{h0} + k_h h + b_h \dot{h}, \tag{2}$$

the dots denoting derivatives with respect to t, and an additional coefficients k_{h0} has been added for completeness. For simplicity, $k_{h0} = 0$ in all the reported calculations. The resulting heaving motion is assumed harmonic with the same frequency of the prescribed pitching motion, with unknown (dimensionless) amplitude h_0 and with a phase lag ϕ with respect to the pitching motion:

$$h(t) = \Re\left[h_0 e^{i(kt+\phi)}\right]. \tag{3}$$

All the amplitudes are assumed small compared with the chord length c, i.e., $\alpha_0 \ll 1$ and $h_0 \ll 1$. Thus, in first approximation, the foil and its wake can be assumed on the plane $z = 0$, with the foil extending from $x = -1$ to

$x = 1$ (see figure 1). The flexibility of the foil is also considered by assuming a sufficiently large stiffness, so that the chordwise flexural deflection amplitude is also small. With these assumptions, we follow Refs. [23, 24] to approximate the deflection $z_s(x,t)$ of the centerline of the foil as a quartic polynomial,

$$z_s(x,t) = h(t) - (x-a)\alpha(t) + (x-a)^2 d(t) - (x-a)^3 \frac{2d(t)}{3(1-a)} + (x-a)^4 \frac{d(t)}{6(1-a)^2}, \tag{4}$$

where the chordwise flexural deflection $d(t)$ around the pivot axis $x = a$ is also assumed a harmonic function,

$$d(t) = \Re\left[d_m e^{i(kt+\psi)}\right], \tag{5}$$

of amplitude $d_m \ll 1$ and phase shift ψ with respect to the prescribed pitching motion (1).

After substituting $z_s(x,t)$ from (4) into the Euler-Bernoulli beam equation and taking the first three moments of this equation one obtains the following three differential equations for the heaving and chordwise flexural deflection motions and for the input torque, $h(t)$, $d(t)$ and $C_{M_i}(t)$, respectively, for given pitching motion $\alpha(t)$ and the structural and kinematic parameters of the foil [23, 24]:

$$m\left[\ddot{h} + (a-x_0)\ddot{\alpha}\right] + J_a\ddot{d} = C_L - C_{L_o}, \tag{6}$$

$$m(x_0-a)\ddot{h} - I_a\ddot{\alpha} + J_d\ddot{d} = 2\left(C_M + C_{M_i} - C_{M_o}\right), \tag{7}$$

$$I_a\ddot{h} - I_d\ddot{\alpha} + K_d\ddot{d} + \frac{16}{3}\frac{a^2+\frac{1}{3}}{(1-a)^2} S\, d = C_F. \tag{8}$$

In this equation, C_L, C_M and C_F are the lift, moment and flexural coefficients, respectively, related to the pressure that the fluid exerts on the foil as

$$C_L(t) = \int_{-1}^{1} \Delta C_p(x,t)dx, \quad C_M(t) = \frac{1}{2}\int_{-1}^{1}(x-a)\Delta C_p(x,t)dx, \quad C_F = \int_{-1}^{1}(x-a)^2\Delta C_p(x,t)dx, \tag{9}$$

where $\Delta C_p(x,t) = (p^- - p^+)/(\rho U^2)$ is the nondimensional pressure difference between the lower and upper sides of the airfoil. When the foil motion (4) is harmonic, with $\alpha(t)$, $h(t)$ and $d(t)$ given by (1), (3) and (5), respectively, these coefficients are given in Appendix A [but written in a general form in terms of $\alpha(t)$, $h(t)$ and $d(t)$]. The system of differential equations (6)-(8) is then transformed into a linear system of complex algebraic equations for the amplitudes h_0 and d_m, the phase shifts ϕ and ψ, and the amplitude and phase of the input torque (see §IV immediately below). The nondimensional stiffness of the foil S and its mass ratio R are defined as

$$S(x) = \frac{E(x)\varepsilon^3(x)}{\rho U^2 c^3}, \quad R(x) = \frac{\rho_s(x)\varepsilon(x)}{\rho c}, \tag{10}$$

where E its elastic modulus of the foil, ρ_s its density, and ε its thickness. These quantities may vary along the chord, but S has been assumed constant in deriving Eqs.(6)-(8) for simplicity (if a stiffness distribution $S(x)$ were used, the term

containing S in (8) would be slightly different and new terms associated to S would appear in the other two equations [23]). However, the mass ratio R has been allowed to vary arbitrarily with x in the remaining coefficients appearing in (6)-(8), which are defined as

$$m = 2\int_{-1}^{1} R dx = 4R, \quad m(x_0 - a) = 2\int_{-1}^{1} (x-a) R dx = -4aR, \qquad x_0 = 2\int_{-1}^{1} xR dx \tag{11}$$

$$I_a = 2\int_{-1}^{1} (x-a)^2 R dx = 4R\left(\frac{1}{3} + a^2\right), \tag{12}$$

$$J_a = 2\int_{-1}^{1} \left[(x-a)^2 - \frac{2}{3}\frac{(x-a)^3}{1-a} + \frac{(x-a)^4}{6(1-a)^2}\right] R dx = 2R\left[a^2 - \frac{2}{3}a - \frac{1}{3} + \frac{16}{15(1-a)^2}\right], \tag{13}$$

$$I_d = 2\int_{-1}^{1} (x-a)^3 R dx = -4Ra\left(1 + a^2\right), \tag{14}$$

$$J_d = 2\int_{-1}^{1} \left[(x-a)^3 - \frac{2}{3}\frac{(x-a)^4}{1-a} + \frac{(x-a)^5}{6(1-a)^2}\right] R dx = 2R\frac{-12 - 93a + 60a^2 - 110a^3 + 120a^4 - 45a^5}{45(1-a)^2}, \tag{15}$$

$$K_d = 2\int_{-1}^{1} \left[(x-a)^4 - \frac{2}{3}\frac{(x-a)^5}{1-a} + \frac{(x-a)^6}{6(1-a)^2}\right] R dx = 2R\frac{141 + 168a + 1281a^2 - 1120a^3 + 1015a^4 - 840a^5 + 315a^6}{315(1-a)^2}, \tag{16}$$

where R is assumed constant in the expressions on the rightmost-hand sides. Some of these nondimensional parameters are the common ones for a rigid foil: the nondimensional mass m, the nondimensional center of mass x_0 and the nondimensional moment of inertia about the pivot point I_a (note that $m(x_0 - a)$ is the nondimensional static moment about $x = a$). The remaining ones, J_a, J_d, I_d and K_d, are dimensionless structural parameters arising from the coupling of the chordwise flexural deflection $d(t)$ with the heaving and pitching motions about the pivot point $x = a$ through the mass ratio distribution $R(x)$. When R is constant, the center of mass is at the center of the foil, $x_0 = 0$. Note that, in general, the pivot point location $x = a$ does not coincide with the center of mass x_0 in the present formulation.

Finally, we have included in Eq. (7) an output moment,

$$C_{Mo} = k_{\alpha 0} - k_\alpha \alpha - b_\alpha \dot{\alpha}, \tag{17}$$

to allow for the possibility that energy can be additionally extracted through a torsional damper with dimensionless constant b_α, including also a torsional spring with dimensionless constant k_α (note that α has been defined positive in the opposite direction of the positive moment), and a dry friction parameter $k_{\alpha 0}$ for completeness. But $C_{M_o} = 0$ in all the reported results.

IV. Analytical solutions

Equations (6) and (8), together with the expressions (A.1), (A.3) and (2) for C_L, C_F and C_{L_o}, respectively, and the kinematics (1), (3) and (5), is a linear system of two algebraic, complex equations for the heave and chordwise deflection amplitudes, h_0 and d_m, as well as for their respective phase lags ϕ and ψ with respect to the imposed pitching motion. These quantities are obtained as a function of the stiffness and mass ratio of the foil, S and $R(x)$, the pitch amplitude

α_0, the centre of mass and pivot point locations, x_0 and a, the spring stiffness, k_h, and, in the energy extraction case, the rest of the coefficients in Eq.(2). Once the heave and flexural deflection are obtained, equation (7), together with (A.2) for C_M and (17) for C_{M_o}, yields the input torque C_{M_i} needed to generate the forced pitching motion (1) and, therefore, the power input and the corresponding efficiency of the system. For the propulsion problem, the thrust force is computed from the prescribed and calculated displacements of the foil, and then the efficiency, which is the power generated by the thrust divided by the power input. In the energy harvesting case, the power output is proportional to C_{L_o} (plus a term related to C_{M_o} if a torsional damper also exists, see below).

From equations (6) and (8), the solution for the heaving and flexural deflection motions is obtained from a linear system of two complex equations which can be formally written as

$$\mathbf{A}\cdot\mathbf{X}=\mathbf{b} \quad \text{with} \quad \mathbf{A}=\begin{pmatrix} A_{11} & A_{12} \\ A_{21} & A_{22} \end{pmatrix}, \quad \mathbf{X}=\begin{pmatrix} \dfrac{h_0 e^{i\phi}}{\alpha_0} \\ \dfrac{d_m e^{i\psi}}{\alpha_0} \end{pmatrix}, \quad \mathbf{b}=\begin{pmatrix} b_1 \\ b_2 \end{pmatrix}, \tag{18}$$

where the different coefficients A_{ij} and b_j, which are given in Appendix B, depend on all the dimensionless parameters but α_0, that due to the linearity of the problemw is absorbed into the solution $\mathbf{X}$ (the heave and flexural amplitudes increase linearly with the amplitude of pitching α_0). The solution can be written as

$$h_0=\alpha_0|B_1|, \quad d_m=\alpha_0|B_2|, \quad \phi=\arg(B_1), \quad \psi=\arg(B_2), \tag{19}$$

where

$$B_1=\frac{A_{12}b_2-A_{22}b_1}{A_{12}A_{21}-A_{11}A_{22}}, \quad B_1=\frac{A_{11}b_2-A_{21}b_1}{A_{12}A_{21}-A_{11}A_{22}}. \tag{20}$$

A. First natural frequency

For a rigid foil in absence of fluid-structure interaction, i.e., assuming $S\to\infty$ and $C_L=C_M=C_F=0$, and considering only the case in which $C_{L_o}=k_h h$ (i.e., the propulsion problem with $b_h=0$), one obtains $d_m=0$ from the second linear equation in (18) and

$$h_0 e^{i\phi}=\frac{m(a-x_0)k^2\alpha_0}{k_h-mk^2}=\frac{4Rak^2\alpha_0}{k_h-4Rk^2}, \tag{21}$$

from the first one, so that $\phi=0$ or $\phi=\pi$ depending on the sign of the right hand side (the rightmost expression is for constant R). From equation (7), the corresponding input torque when $C_{M_0}=0$ is

$$C_{M_i}=\Re[C_i e^{ikt}], \quad C_i=\frac{k^2 h_0}{2}\left[I_a+\frac{m^2(a-x_0)^2k^2}{k_h-mk^2}\right]. \tag{22}$$

The value of k for which the denominator in (21) vanishes is the nondimensional frequency of the first (and only one with the present approximation) resonant mode of the airfoil, which now consists of just a rigid plate attached to a

spring of stiffness k_h, with the well-know resonant frequency

$$k_{r0} = \sqrt{\frac{k_h}{m}} = \sqrt{\frac{k_h}{4R}}, \tag{23}$$

the right-most expression valid for constant R. Note that this resonant frequency is independent of the pivot point location.

Still neglecting the FSI, but when the foil is flexible, with a finite stiffness S, and when the passive heave is inhibited by a spring of infinite stiffness ($k_h \to \infty$), the first linear equation in (18) yields $h_0 = 0$, and from the second equation results

$$d_m e^{i\psi} = \frac{I_d k^2 \alpha_0}{\dfrac{16(a^2+1/3)}{3(1-a)^2} S - K_d k^2}. \tag{24}$$

Thus, the resonant frequency in this case is

$$k_{r0} = \sqrt{\frac{16(a^2+1/3)S}{3(1-a)^2 K_d}} = \sqrt{\frac{280(1+3a^2)S}{(141+168a+1281a^2-1120a^3+1015a^4-840a^5+315a^6)R}}. \tag{25}$$

This expression for the resonant frequency obviously coincides with that in [24] for a passive pitching motion in the limit $k_\alpha \to \infty$, but the deflection (24) does not.

For a flexible airfoil with passive heaving through a spring of finite stiffness k_h, but still neglecting the FSI (and with $C_{L_o} = k_h h$), the nondimensional, first natural frequency can be obtained form $\det(\mathbf{A}) = 0$; i.e., from the positive root of

$$k_{r0}^2 = \frac{mS^* + K_d k_h + \sqrt{(mS^* + K_d k_h)^2 - 4k_h S^*(mK_d - I_a J_a)}}{2(mK_d - I_a J_a)}, \quad S^* = \frac{16}{3}\frac{a^2+\dfrac{1}{3}}{(1-a)^2} S. \tag{26}$$

Finally, when the fluid-structure interaction is taken into consideration, i.e., when solving (18) taking into account the effect of C_L and C_F, $\mathbf{A}$ ceases to be real, even for the case of a rigid airfoil, and there is no proper resonant frequency for which h_0 (and/or d_m) becomes singular. However, there exists a frequency that maximizes the passive heave (and/or the deflection amplitude), and, as we shall see in §V below, will maximize also the thrust force for each set of nondimensional parameters. At this frequency, corresponding to the minimum value of $|\det(\mathbf{A})|$ and dubbed as $k = k_r$, the maximum of h_0 (and/or d_m) is usually quite large, so it may still be called the resonant or natural frequency [32]. Clearly, k_r tends the resonant frequency *in vacuo* k_{r0} for $R \to \infty$, as the FSI becomes negligible (see results in §V, where the different limits for k_{r0} are considered).

B. Input power

Once the linear system (18) is solved, equation (7) yields the required input torque C_{M_i}, and hence the input power coefficient:

$$C_{P_i}(t) = -2\dot{\alpha}(t) C_{M_i}(t). \tag{27}$$

Note from equation (7) that this expression coincides with the usual one $C_{P_i} = 2\dot{\alpha}(t)C_M(t)$ for the propulsion of a pitching foil only for very small mass ratios ($R \to 0$) and provided that $C_{M_o} = 0$ (propulsion problem).

The time-averaged input power coefficient, defined as

$$\overline{C}_{P_i} = \frac{k}{2\pi}\int_t^{t+2\pi/k} C_{P_i}(t)dt\,, \tag{28}$$

can be written as a sum of several terms:

$$\overline{C}_{P_i} = -2\overline{\dot{\alpha}C_{M_i}} = \overline{C}^0_{P_i} + \overline{C}^d_{P_i} + \overline{C}^m_{P_i} + \overline{C}_{P_{o\alpha}}\,. \tag{29}$$

$\overline{C}^0_{Pi}$ is the FSI contribution from the terms in C_M associated to the motion of the foil as a rigid body,

$$\overline{C}^0_{Pi} = -\pi k\alpha_0^2\left[\left(\frac{1}{4}-a^2\right)k\mathcal{F} - \frac{k}{2}\left(\frac{1}{2}-a\right) + \left(a+\frac{1}{2}\right)\mathcal{G}\right] - \pi k^2 h_0\alpha_0\left\{-\left(a+\frac{1}{2}\right)\mathcal{F}\cos\phi + \left[\left(a+\frac{1}{2}\right)\mathcal{G} + \frac{ak}{2}\right]\sin\phi\right\}. \tag{30}$$

This contribution obviously coincides with Theodorsen's power coefficient for a rigid foil when only the terms coming from C_M are considered [33, 34] (but with the phase lag ϕ now in the heaving motion), where $\mathcal{F}$ and $\mathcal{G}$ are the real and imaginary parts of Theodorsen's function C defined in equation (A.5) in Appendix A. The contribution of the flexural deflection motion of the airfoil associated to the FSI (i.e., from the terms with $d(t)$ in C_M), is

$$\overline{C}^d_{Pi} = \pi k\alpha_0 d_m\left\{\left[\left(a+\frac{1}{2}\right)(A_{g1}k\mathcal{F} + A_{g0}\mathcal{G}) + \frac{A_{m1}k}{2}\right]\cos\psi - \left[\frac{1}{2}(A_{m2}k^2 - A_{m0}) + \left(a+\frac{1}{2}\right)(A_{g1}k\mathcal{G} - A_{g0}\mathcal{F})\right]\sin\psi\right\}, \tag{31}$$

where the different functions of a, A_{m0}, A_{m1}, A_{m2}, A_{g0} and A_{g1}, are defined in Eqs. (A.6)-(A.10) in Appendix A. The contribution from the inertia of the airfoil, $\overline{C}^m_{Pi}$, is

$$\overline{C}^m_{Pi} = \frac{k^3\alpha_0}{2}\left[m(x_0-a)h_0\sin\phi + J_d d_m\sin\psi\right]\,. \tag{32}$$

Finally, $\overline{C}_{Poh}$, appearing only in the energy harvesting problem, is the contribution from C_{M_o} (it coincides with one of the contributions to the power output, see below):

$$\overline{C}_{P_{o\alpha}} = b_\alpha k^2\alpha_0^2\,. \tag{33}$$

C. Propulsion problem

In this case $b_h = 0$ and $C_{M_0} = 0$, and the propulsion coefficient $C_T(t)$ is obtained from the resulting heaving and chordwise deflection motions, $h(t)$ and $d(t)$, respectively, and the given pitching kinematics $\alpha(t)$. Its time-averaged value can be written as [22, 24]:

$$\overline{C}_T = t_h(k)(kh_0)^2 + t_{hp}(k,a,\phi)kh_0\alpha_0 + t_p(k,a)\alpha_0^2 + t_{dh}(k,a,\psi)kh_0 d_m + t_{pd}(k,a,\psi,\phi)\alpha_0 d_m + t_d(k,a)d_m^2\,, \tag{34}$$

where the functions $t_h(k)$, $t_{hp}(k,a,\phi)$, $t_p(k,a)$, $t_{dh}(k,a,\psi)$, $t_{pd}(k,a,\phi,\psi)$ and $t_d(k,a)$ are given in Appendix C. The propulsion (Froude) efficiency is given by

$$\eta_p = \frac{\overline{C}_T}{\overline{C}_{Pi}} \,. \tag{35}$$

D. Energy harvesting problem

Assuming that all the loss of mechanical energy in the torsional and linear dampers is converted into electric energy, the nondimensional time-averaged power output can be written as

$$\overline{C}_{P_o} = \overline{C}_{Poh} + \overline{C}_{Po\alpha} = \overline{\dot{h}C_{Lo}} - 2\overline{\dot{\alpha}C_{Mo}} = b_h\overline{\dot{h}^2} + 2b_\alpha\overline{\dot{\alpha}^2} = k^2\left[\frac{b_h}{2}h_0^2 + b_\alpha\alpha_0^2\right] . \tag{36}$$

The oscillating foil works as an energy harvester for positive net power output $\overline{C}_{Po} - \overline{C}_{Pi}$. Thus, the energy harvesting (Betz) efficiency can be defined as [13, 14]

$$\eta_e = \frac{\overline{C}_{P_o} - \overline{C}_{P_i}}{h_0 + (1+|a|)\alpha_0 + d_m}, \tag{37}$$

being the fraction of the incoming flow kinematic energy flux (i.e., $\rho U^3 b\Delta/2$) extracted by the system, where $\Delta = (h_0+(1+|a|)\alpha_0+d_m)c$ is the maximum of the total distance that can be swept by any portion of the foil. The normalized quantity

$$\hat{\eta}_e = \frac{\eta_e}{\alpha_0}, \tag{38}$$

will be used in all the reported results because, in the present linear theory, it is independent of the pitch amplitude α_0, and therefore the efficiency results in terms of $\hat{\eta}_e$ are more general. However, it is not an efficiency properly because it could be larger than unity. To compare with results reported in the literature one has just to multiplying by the prescribed (and small) α_0.

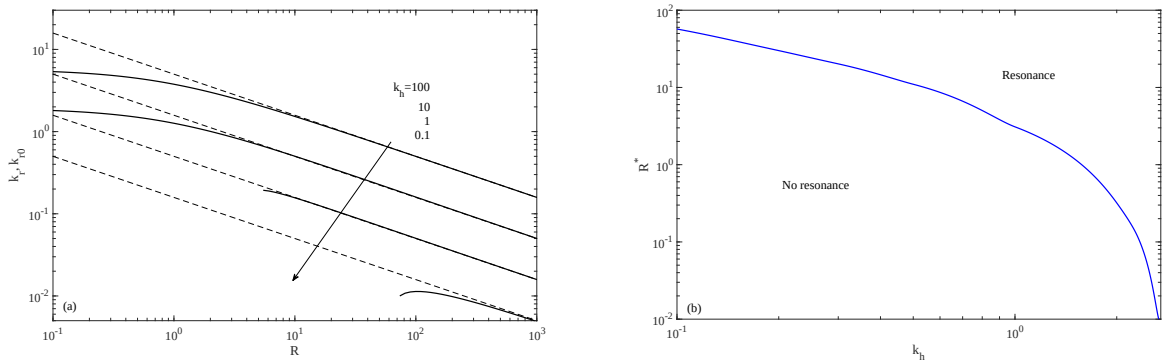

Fig. 2 (a): k_r that minimizes $|A_{11}|$ vs. R (solid lines) and k_{r0} given by (23) (dashed lines) for some k_h. (b): R^* vs. k_h.

V. Results

A. Propulsion of a pitching rigid airfoil with passive heaving

We consider first the propulsion problem ($C_{M_o} = 0$ and $b_h = 0$) of a rigid airfoil ($S \to \infty$) with constant R (i.e., $x_0 = 0$). This problem has been analyzed previously by Murray and Howle [8] and by Mackowski and Williamson [9]. Equation (8) is not needed in this rigid foil limit ($d_m = 0$) and Eq. (18) reduces to

$$A_{11}\frac{h_0}{\alpha_0}e^{i\phi} = b_1\,; \quad \text{i.e.,} \quad \frac{h_0}{\alpha_0} = \left|\frac{b_1}{A_{11}}\right| \quad \text{and} \quad \phi = \arg\left(\frac{b_1}{A_{11}}\right). \tag{39}$$

For large R, when the FSI can be neglected, $|A_{11}|$ vanishes at the first resonant frequency given by Eq. (23), and the heave amplitude h_0 becomes infinite. When the FSI is considered, the heave amplitude is not singular, but reaches a maximum values at the natural frequency k_r that minimizes $|A_{11}|$. As shown in figure 2(a), where k_r, together with k_{r0} from (23), are plotted vs. R for several values of k_h, this resonant frequency only exists for $R > R^*$, where R^* depends only on the spring stiffness k_h. This function $R^*(k_h)$ is plotted in Fig. 2(b). It is observed that for k_h smaller than about unity, R^* is quite large, so that when k_r exists it practically coincides with the value k_{r0}. As k_h increases, resonance exists for an increasingly range of mass ratios R, so that the resulting enhancement of heaving amplitude can be useful in a wider range of configurations, including both air and aquatic flapping propulsion. For $k_h \gtrsim 2.5$, k_r exists for any value of R (i.e., $R^* \simeq 0$).

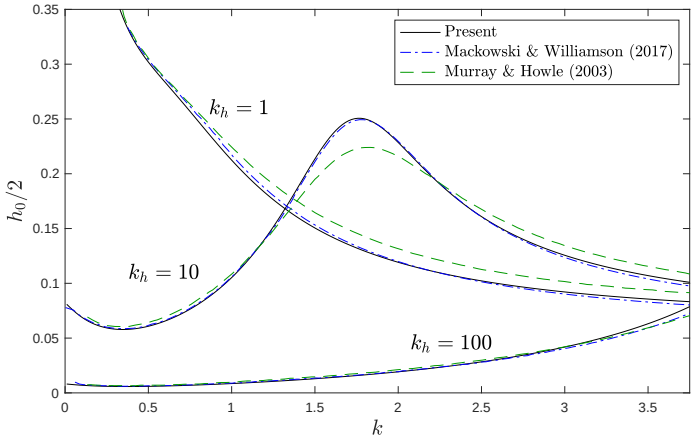

Fig. 3 Comparison of the present theoretical results with numerical ones by Murray and Howley [8] and by Mackowski and Williamson [9] (from figure 5 in Ref. [9]). $\alpha_0 = 15^o$**,** $a = -1/2$**,** $x_0 = 0$**,** $R = 0.1$**, and** $k_h = 1$**,** 10 **and** 100**.**

To validate the present theoretical results for the passive heave amplitude h_0 from Eq. (39) we compare them with previous numerical results by Murray and Howley [8] for several values of the spring stiffness k_h pivoting at the quarter-chord point (figure 3), and with experimental data for different pivot point locations from Mackowski and Williamson [9] (figure 4). In figure 3, in addition to the numerical results by Murray and Howley [8] based on an unsteady, two-dimensional vortex lattice method, we also include results by Mackowski and Williamson [9] from an iterative approximate method to solve the linear dynamic equations with Theodorsen's lift. The data and the values of the different parameters are taken from figure 5 of Ref. [9], where the heave amplitude scaled with the chord ($h_0/2$ in

the present notation) is plotted. We see good agreement between the three calculations.

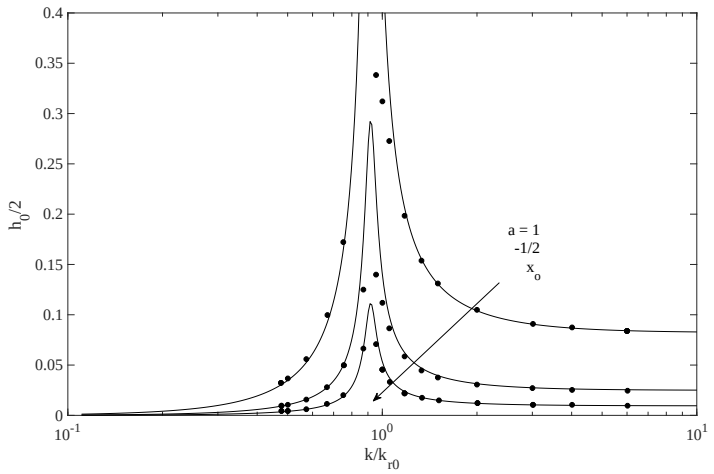

Fig. 4 Comparison between experimental data from Mackowski and Williamson [9] (dots; from figure 14 in Ref. [9]) and present theoretical results (lines) for the heave amplitude vs. k/k_{r0}.

Figure 4 compares the present FSI results for the passive heave amplitude h_0 with experimental data by Mackowski and Williamson [9]. These authors consider in their figure 14 results for a NACA0012 airfoil of constant density ($m^* = 40$ in Ref. [9] is $\rho_s/\rho = 40$ in the present notation), so that its centre of mass coincides with the centroid ($x_0 = -0.159$ in the present notation), actuated at a constant frequency $k = 2$ and Reynolds number 1.7×10^4, for several pivot point locations a. They measure the heave amplitude scaled with the chord ($h_0/2$ in the present notation) as a function of $f^* = k/k_{r0}$ by varying the spring constant k_h in $k_{r0} = \sqrt{k_h/m}$. The theoretical results plotted in figure 4 are obtained using $m = 4R = 4m^*\varepsilon/c = 16$, assuming a constant thickness $\varepsilon/c = 0.1$. In spite of these simplifications, the agreement with the experimental results is quite remarkable, considering that h_0 is obtained here from just the algebraic equation (39), that accounts for the FSI. Clearly, the heave amplitude h_0 presents a pronounced maximum at the natural frequency k_r, which is almost independent of a and, for the values of the remaining parameters in figure 4, very close to k_{r0}, just a bit smaller ($k_r/k_{r0} \simeq 0.92$), as also observed in figure 2. The theory predicts very accurately this resonant frequency, and the heave amplitude in general, except close to k_r, where it overpredicts the peak amplitude.

At these resonant frequencies where the heave amplitude undergoes such a remarkable peak there also exists a great amplification of the thrust with respect to its value for a purely pitching motion of the airfoil, $\overline{C}_T - \overline{C}_T^0$, as shown in figure 5(a) for a foil with $R = 1$ pivoting at the leading edge ($a = -1$) and two spring stiffnesses k_h (the plotted results are do not depend of the pitching amplitude α_0 since $\overline{C}_T \propto \alpha_0^2$ in the present linear theory). Clearly, the present results coincide with those for a purely pitching motion when $k_h \to \infty$. At the resonant frequencies there is also a marked enhancement of the input power required to pitch the foil, so that the efficiency (35) does not, in general, presents a maximum, as it actually happens for the cases shown in figure 5, where η_p is always smaller that η_p^0 for a pitching foil [see figure 5(b)]. At $k = k_r$, the efficiency is just a bit smaller, so that at resonance one gets a large thrust force amplification through passive heave but with practically the same propulsive efficiency of a purely pitching motion.

Since the main gain of adding passive heave is in thrust enhancement, rather than in efficiency enhancement,

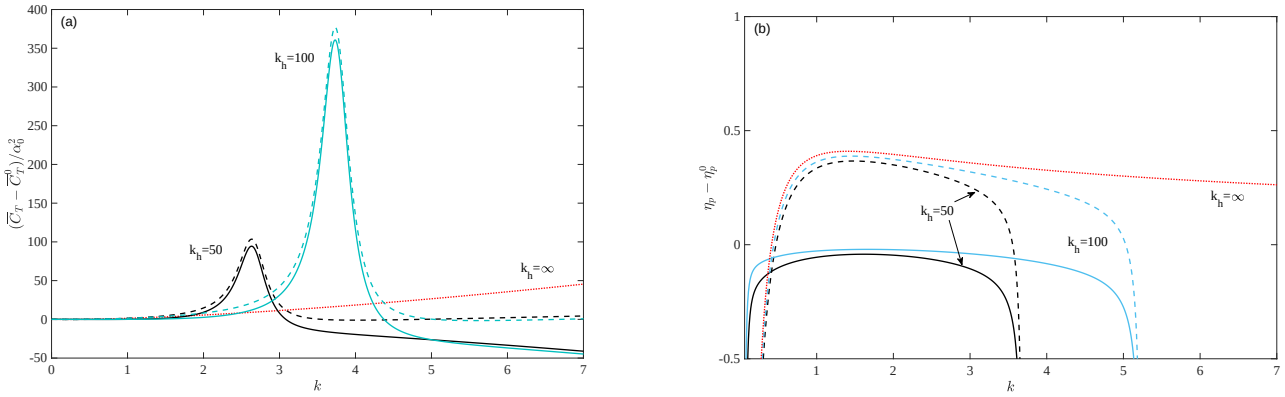

Fig. 5 $(\overline{C}_T - \overline{C}_T^0)/\alpha_0^2$ **(a) and** $\eta_p - \eta_p^0$ **(b) vs.** k **for rigid foils with** $R = 1$, $a = -1$ **and several** k_h **(continuous lines). Dashed lines correspond to** $\overline{C}_T$ **and** η_p **and dotted lines to purely pitching motions,** $\overline{C}_T^0$ **and** η_p^0**.**

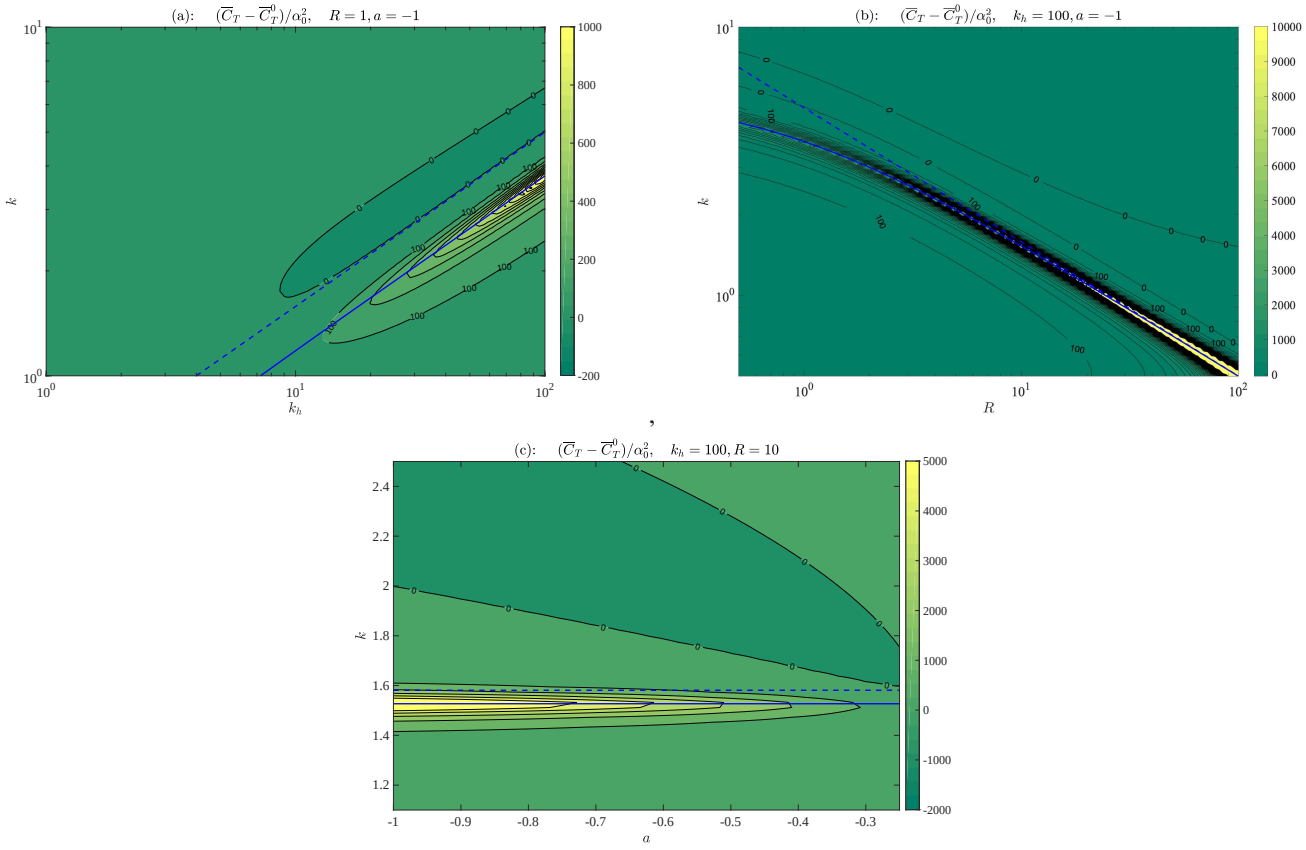

Fig. 6 Thrust enhancement of a rigid airfoil in the $k_h - k$ **plane for** $R = 1$ **and** $a = -1$ **(a), in the** $R - k$ **plane for** $k_h = 100$ **and** $a = -1$ **(b), and in the** $a - k$ **plane for** $k_h = 100$ **and** $R = 10$ **(c). Contours 0' indicate where the passively heaving airfoil has the same thrust as the equivalent pitching-only airfoil with** $k_h \to \infty$ **(i.e.,** $\overline{C}_T^0$**). The thick continuous lines correspond to** $k = k_r$ **that minimizes** $|A_{11}|$ **and the dashed lines to** k_{r0} **given by Eq.** (23)**.**

figure 6 shows only contours plots of $(\overline{C}_T - \overline{C}_T^0)/\alpha_0^2$ as k, R, k_h and a are varied. These results show that the thrust enhancement grows as k_h or R increases, and when the pivot point approaches the leading edge ($a = -1$). In all cases, the maximum thrust enhancement is observed very close to the natural frequency k_r that minimizes $|A_{11}|$, shown in figure 6 as continuous lines, while the first natural frequency *in vacuo* k_{r0} given by Eq. (23), plotted with dashed lines,

yields a good estimation of the upper frequency limit above which no thrust enhancement is achieved for any value of the parameters. In particular, it is observed in figure 6(c) that the frequency for the maximum thrust enhancement is practically independent of the pivot point location a, in accordance with k_r (and k_{r0}). Also observed in this last subfigure is that no significant thrust enhancement is produced when pivoting downstream of, approximately, the quarter chord point ($a \gtrsim -1/2$). Finally, it is worth noticing that the fact that large thrust enhancement is only predicted for R larger than unity makes this passively heaving rigid flapping foil system more appropriate for aerial, rather than for aquatic, propulsion. The more so, the larger R.

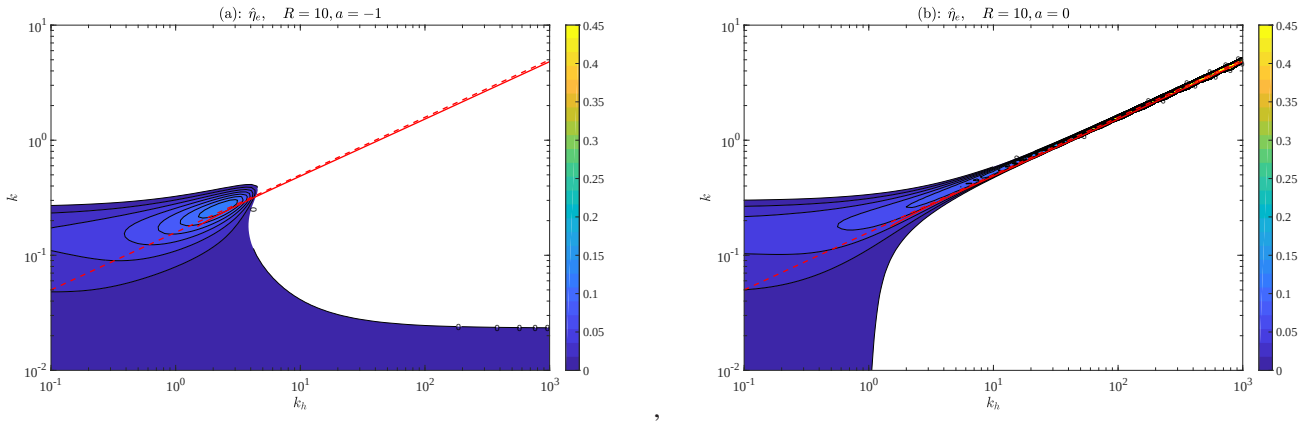

Fig. 7 $\hat{\eta}_e$ **vs.** k **and** k_h **for a rigid airfoil with** $R = 10$ **for** $a = -1$ **(a) and** $a = 0$ **(b).** $b_h = 1$ **and** $b_\alpha = 0$**. Only regions with** $\hat{\eta}_e \geq 0$ **are plotted. Continuous lines correspond to** k_r**, dashed lines to** k_{r0} **given by Eq.** (23)**.**

B. Energy harvesting from a pitching rigid airfoil with passive heaving

To characterize the effect of passive heave on the energy harvested by a pitching rigid airfoil ($S \to \infty$) only the case in which the energy is extracted by the linear damper ($b_\alpha = 0$) is considered, setting $b_h = 1$ and assuming also constant R ($x_0 = 0$).

Maxima in the energy harvesting efficiency $\hat{\eta}_e$ are also found close to the resonant frequency k_r that minimizes $|A_{11}|$ for a given set of parameters, as it happens for the thrust enhancement considered above, but now $\hat{\eta}_e$ is found positive only when R is larger than about unity. In fact, for sufficiently large R, figure 7 (for $R = 10$) shows that, as the spring stiffness k_h is varied, there exists two regimes where energy can be harvested: one for low frequencies and low spring stiffnesses when the pivot point location is at, or near, the leading edge [$a = -1$ in figure 7(a)], and the other one for large k and k_h when the pivot is close to the mid-chord point [$a = 0$ in figure 7(b)]. In both cases the local maxima are close to k_r ($\simeq k_{r0}$ when R is large, both natural frequencies shown in the figure), but in (a) the local maximum of $\hat{\eta}_e$ is located in the low stiffness limit of k_r, just before ceasing to exists (see figure 2), while in (b) local maxima of $\hat{\eta}_e$ exist in a narrow band around the high stiffness range of k_r. The energy harvesting efficiency in the first case is lower than in the second, but remains sufficiently high in a much broader region of the frequency - stiffness plane. In the second case, higher values of $\hat{\eta}_e$ can be achieved, but in a very narrow band around $k = k_r(k_h)$ for high frequencies and stiffnesses.

Since we know that the peaks of energy harvesting efficiency are clearly overpredicted by the present linear theory

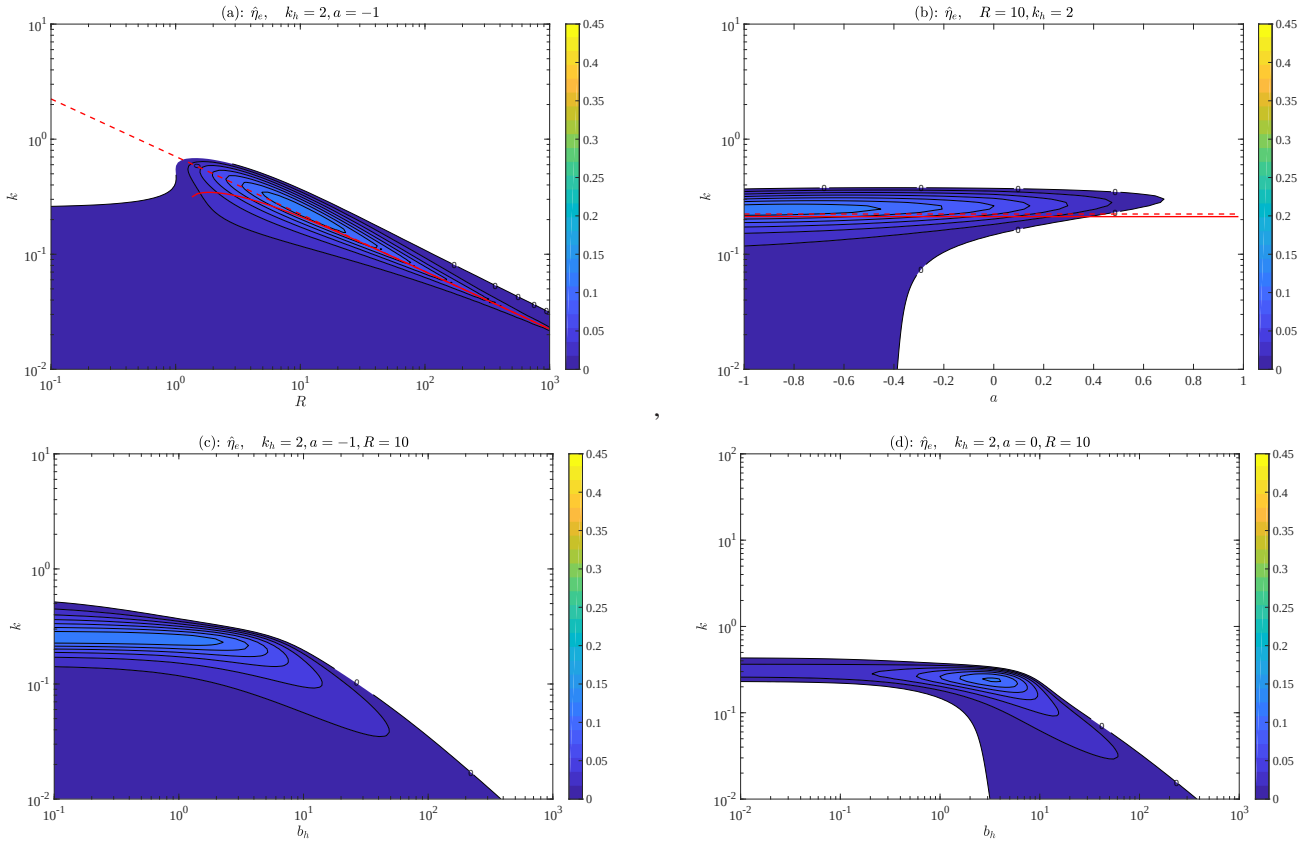

Fig. 8 (a) and (b): As in figure 7 but with contours of $\hat{\eta}_e$ in the $R - k$ plane for $k_h = 2$ and $a = -1$ in (a), and in the $a - k$ plane for $k_h = 2$ and $R = 10$ in (b). All with $b_h = 1$. (c): Contours of $\hat{\eta}_e$ in the $b_h - k$ plane for $k_h = 2$, $R = 10$ and $a = -1$. (d): As in (c), but for $a = 0$.

for sufficiently large values of k_h, as it happens with the heave amplitude (see figure 4) and with the thrust enhancement, we consider here only the first region of positive energy harvesting efficiency depicted in figure 7(a). (The second region is also limited to pivots very close to the mid-chord point and values of R in a very narrow band for every $k = k_r$.) Figures 8(a) and (b) show the regions of positive $\hat{\eta}_e$ in the $R - k$ plane and in the $a - k$ plane, respectively, for optimal values of the remaining parameters. We see that, for frequencies close to the natural frequency k_r, the optimal values of R for energy harvesting are of order of ten when the pivot point is located at, or close to, the leading edge. In any case, for pivot points downstream of the mid-chord point no energy can be harvested by the rigid pitching foil with passive heave in this low frequency range according to the present theory [Fig. 8(b)].

All these results are for a damping coefficient $b_h = 1$. Figure 8(c) shows the contours of $\hat{\eta}_e$ in the $b_h - k$ plane for roughly the optimal values of the remaining parameters, namely $R = 10$, $a = -1$ and $k_h = 2$. It is observed that the local maxima of the efficiency are practically independent of b_h provided that b_h is smaller than about 2, and that the optimal frequency remains almost constant around $k = 0.25$, as also observed in figure 8(b) when the pivot point location is varied. This is a consequence of the fact that k_r is almost independent of a and b_h [actually, k_{r0} given by Eq. (23) does not depend on these two parameters, and $k_r \simeq k_{r0}$ for $R = 10$]. These optimal values and ranges of the different parameters are in qualitative agreement with those found by Ma et al. [21] in their numerical study on the performance of a semi-passive oscillating foil, thought these authors found that the maximum energy harvesting

efficiency is obtained at a pitching amplitude $\alpha_0 = 85^o$, which is obviously far away from the validity range of the present linear theory. (Remember that $\hat{\eta}_e$ is independent of α_0 in the present theory, and that the actual efficiency is easily obtained by just multiplying it by the prescribed pitch amplitude). On the other hand, that the efficiency remains the same across a large range of b_h in figure 8(c) is due to the fact that the pivot point is at the leading edge ($a = -1$). Figure 8(d) shows the efficiency for the same configuration used in figure 8(c) except for the pivot point located at the mid-chord ($a = 0$), showing a maximum at $b_h \approx 3$, in qualitative agreement with the findings of Su and Breuer [20] for the same pivot location, but with other values of the remaining parameters. (Incidentally, it is observed that $a = -1$ gives slightly better energy harvesting performance than $a = 0$ in this low frequency and low stiffness range.) Although the experimental study of Su and Breuer [20] is for a pitch amplitude $\alpha_0 = 65^o$, far from the validity range of the linear theory, the results from the present formulation plotted in figure 9 reproduce quite well the pattern of their experimental data for the heave amplitude and the efficiency in the frequency ratio - damping coefficient plane. Note that their f/f_n and b^* are k/k_{r0} and b_h in the present notation, respectively, and that their mass ratio is $m^* = 2R$. $\hat{\eta}_e$ with $b_\alpha = 0$ is a heave efficiency, and it is plotted in figure 9(b) without subtracting the input power $\overline{C}_{P_i}$ in (37), as it is defined in [20]. Both magnitudes plotted in figure 9 are normalized with the prescribed pitch amplitude, and therefore independent of α_0 in the present formulation.

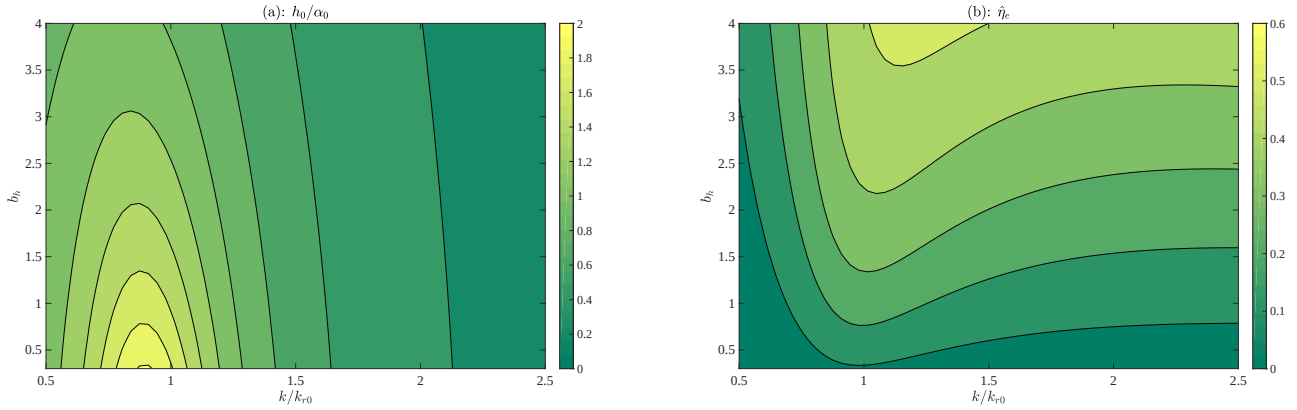

Fig. 9 Normalized heave amplitude (a) and efficiency (see main text) (b) in the $k/k_{r0} - b_h$ plane for $b_\alpha = 0$, $a = 0$ and $R = 2.45$, to compare with experimental data in figures 3(a) and 3(f) of Ref. [20].

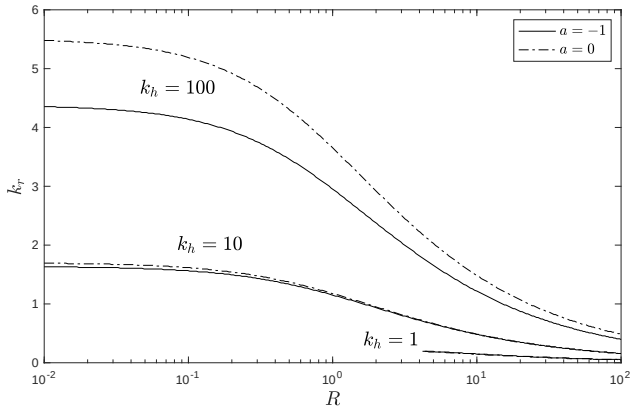

Fig. 10 k_r that minimizes $|\det(\mathbf{A})|$ vs. R for $S = 100$, three values of k_h and two values of a.

C. Propulsion of a pitching airfoil with passive heaving and chordwise flexibility

The effect of chordwise flexibility in the propulsion problem is considered here. Now, both equations (6) and (8) have to be solved simultaneously to obtain the heave and chordwise flexural deflection amplitudes and phases, given by equations (18)-(20). Contrary to what happens in the rigid-foil case ($S \to \infty$), the first natural frequency $k = k_r$ that minimizes $|\det(\mathbf{A})|$ now depends on the pivot axis location a, but this dependency is only relevant for sufficiently large spring stiffness k_h, as shown in figure 10 for $S = 100$.

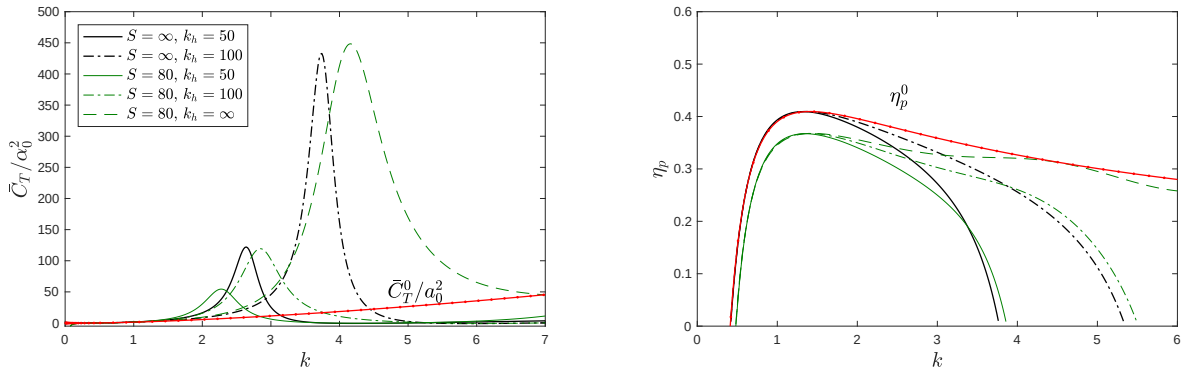

Fig. 11 Normalized thrust (a) and efficiency (b) vs. k for $R = 1$, $a = -1$ and several values of S and k_h. Red lines with dots are for rigid foils with a pure pitching motion ($\overline{C}_T^0$ and η_P^0 for $S \to \infty$ and $k_h \to \infty$).

At these resonant frequencies, the thrust $\overline{C}_T$ is amplified, as before, in relation to its value for a pitching-only rigid foil $\overline{C}_T^0$. But, as shown in figure 11 for $S = 80$, this thrust augmentation is smaller than that for a rigid foil with the same spring stiffness k_h. In addition, the propulsive efficiency at these frequencies is also slightly smaller than in the limit $S \to \infty$ for the same k_h.

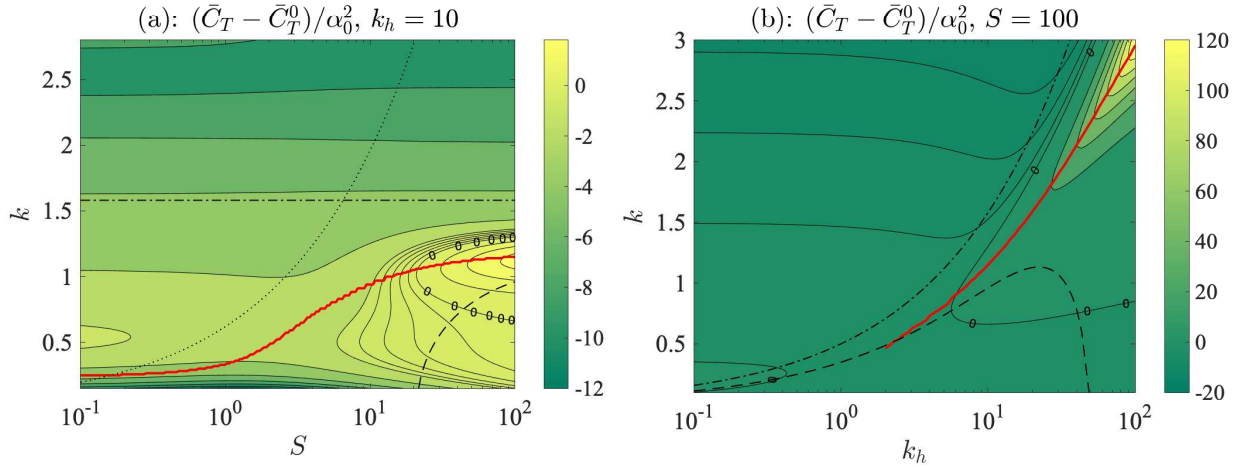

Fig. 12 Contours of thrust enhancement in the $S - k$ plane (a) and in the $k_h - k$ plane (b) for $R = 1$ and $a = -1$. Continuous lines correspond to $k = k_r$ minimizing $|\det(\mathbf{A})|$, dashed-and-dotted lines to k_{r0} given by (23), dotted lines to (25), and dashed lines to (26).

Similar behaviors are observed for other values of S and in k_h. Figure 12 maps the thrust enhancement in the $S - k$ and in the $k_h - k$ planes, respectively, for given values of k_h and S, and for the same values of R and a of figure 11. In both planes the maximum thrust amplification is reached around the first resonant frequency of the system $k = k_r$ that

minimizes $|\det(\mathbf{A})|$, and this magnification is larger as S, or k_h, increases. This situation is somewhat analogous to that found for an airfoil with forced heaving and passive pitching [24, 30]: now it is found that a rigid foil pivoting about its leading edge for given k_h may generate substantially more thrust at a given frequency than any flexible foil for any S; also, for a given spring stiffness k_h, the maximum thrust enhancement is obtained for a rigid airfoil ($S \to \infty$). However, the thrust magnification at the natural frequency is not accompanied by an improvement in the efficiency. The highest thrust amplification is attained along the lower frequency natural mode associated to k_h, which also depends on the flexibility of the plate when the FSI is taken into account. The corresponding optimal frequency is always below the resonant frequency k_{r0} given by Eq. (23), also shown in figure 12 with dashed-and-dotted lines. In other words, for a given operating frequency, the optimal spring stiffness is always larger than that given by Eq. (23). This behavior of the optimal thrust enhancement may be explained by the fact that it is associated to the maxima in the passive heave amplitude rather than the flexural deflection amplitude, as shown in figure 13, where the relative heave and flexural amplitudes are plotted for the same case considered in figure 12(a). The optimal thrust is associated to the natural spring modes rather than to the bending modes, so that adding flexibility to the foil does not improve the propulsive performance for given k_h.

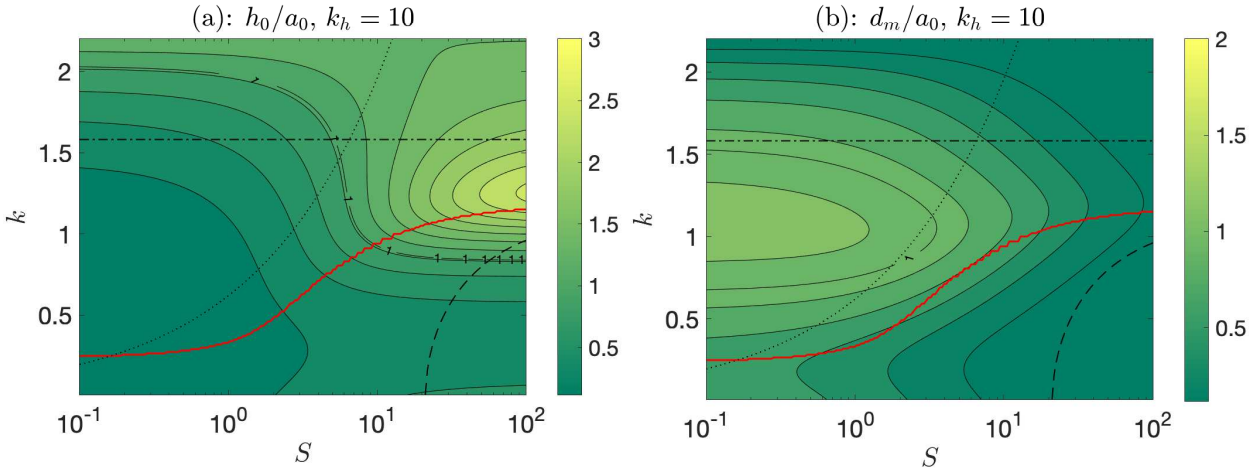

Fig. 13 Contours of relative heave (a) and flexural deflection (b) amplitudes in the $S - k$ plane for the same case plotted in figure 12(a).

Figures 11 and 12 are for $a = -1$ and $R = 1$. In order to appreciate how the pivot axis and the mass ratio affect to the propulsion performance, figure 14 shows the thrust enhancement in the pivot axis-mass ratio plane at the resonant frequencies $k_r(a, R)$ for given values of the stiffnesses of the airfoil and the spring ($S = 100$ and $k_h = 10$, respectively). As shown in figure 10, k_r is almost independent of a for these values of k_h and S. For given R, figure 14 shows that the maximum thrust amplification is obtained when the foil pivots at the leading edge, being positive for $R \geq 0.043$ and increasing monotonically with R.

D. Energy harvesting of a pitching airfoil with passive heaving and chordwise flexibility

Finally, to analyze the effect of flexibility on the energy harvesting performance of the pitching airfoil with passive heave, the most favorable case considered in §V.B for a rigid airfoil (see figures 7 and 8) is considered here. Figure

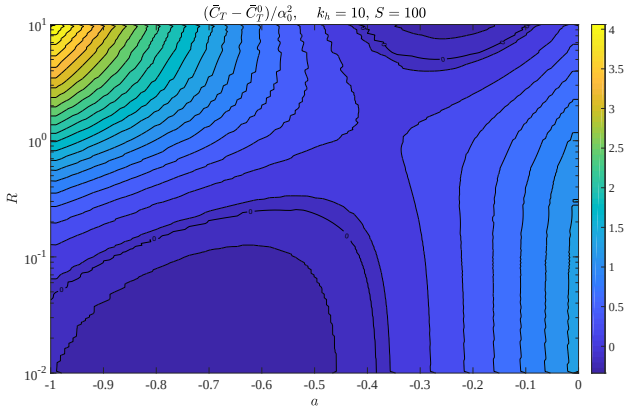

Fig. 14 Contours of thrust enhancement in the $a - R$ plane at the resonant frequency $k = k_r(a, R)$ minimizing $|\det(\mathbf{A})|$ when $S = 100$ and $k_h = 10$.

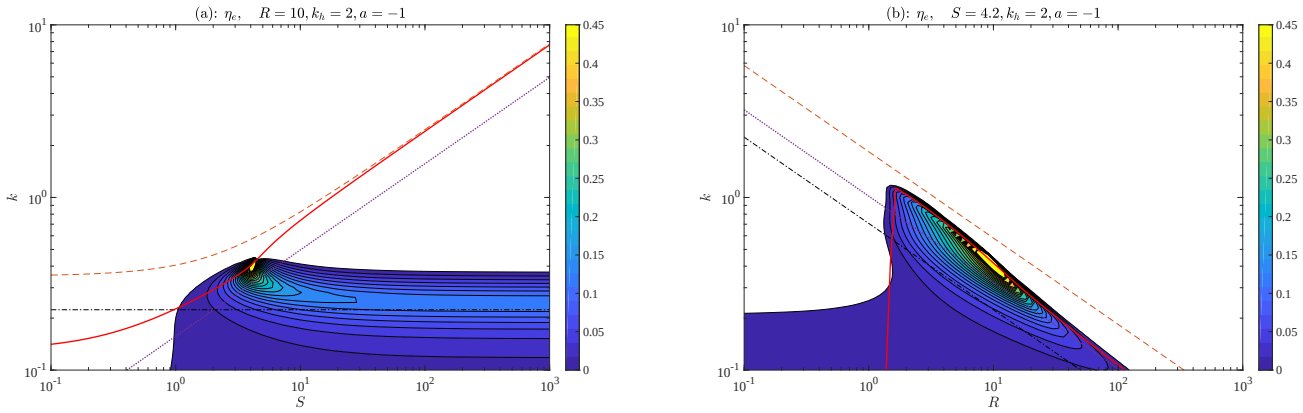

Fig. 15 (a): $\hat{\eta}_e$ as a function of S and k for $R = 10$, $k_h = 2$ and $a = -1$. $b_h = 1$ and $b_\alpha = 0$. (b): Similar to (a), but in the $R - k$ plane with $S = 4.2$. Red continuous lines are for the first natural frequency k_r that minimizes $|\det(\mathbf{A})|$, dashed-and-dotted lines to (23), dotted lines to (25) and dashed lines to (26). Only regions with $\hat{\eta}_e \geq 0$ are plotted.

15(a) shows the efficiency for a pivot axis at the leading edge ($a = -1$) in the stiffness-frequency plane for $k_h = 2$ and $R = 10$ (the energy is only harvested by the linear damper with $b_h = 1$, and $b_\alpha = 0$ as in all the previous cases). The efficiency shows a marked maximum for a stiffness $S \approx 4.2$ when $k \approx 0.4$. For this value of S, figure 15(b) shows how $\hat{\eta}_e$ varies in the mass ratio-frequency plane for the same values of k_h, b_h and a, corroborating that the maximum efficiency is achieved for a mass ratio $R \approx 10$. Note that the maxima of $\hat{\eta}_e$ in figures 15(a) and (b) are significantly larger than for the rigid-foil counterparts plotted in figures 7(a) and 8(a), respectively: about 0.45 in figures 15(a) and (b) vs. approximately 0.15 in figures 7(a) and 8(a). This is a consequence of the enhancement of the passive heave amplitude at the resonant frequencies due to the flexural deflection of the foil for these values of the structural parameters. After exploring other parameter ranges, it is found that the optimal energy harvesting efficiency is reached in the present linear limit for these values of the parameters ($k_h \approx 2$, $R \approx 10$, $S \approx 4$, $a = -1$, $b_h \approx 1$) when operating at a reduced frequency $k \approx 0.4$.

Figure 15 also shows that the resonant frequency k_{r0} *in vacuo* given by Eq. (23), plotted with dashed-and-dotted lines, yields a good estimate for the threshold frequency above which energy can be extracted from a given current and

airfoil parameters.

VI. Conclusions

The fluid-structure interaction of a flexible airfoil with prescribed sinusoidal pitching motion and with passive heave and chordwise flexural deflection has been analysed for any pivot axis from the Euler-Bernoulli beam equation coupled with fluid forces and torques resulting from the vortical impulse theory in the linear inviscid limit. The problem is governed by just a system of three complex, algebraic linear equations. Two of them provide the heave amplitude and its phase-lag, and the flexural amplitude and its phase-lag, with the absolute value of its denominator determinant yielding the (first) resonant frequency of the airfoil-fluid system. The third equation determines, also in closed simple form, the input torque that generates the prescribed pitching, and hence the power input needed to compute the efficiency. The problem is formulated in such a way that the performance of a flapping-foil thruster and a flapping-foil turbine, both with passive heave and deformation, can be analysed with the same set of equations by just selecting the appropriate values of the dimensionless parameters. The maximum energy harvesting efficiency and the maximum thrust in the propulsion configuration are always found at, or close to, the first natural mode of the system, but the optimal propulsive efficiency is not necessary related to this natural frequency.

The present results for the propulsion of a rigid airfoil agree quite well with previous numerical results by Murray and Howle [8] when the pivot axis is at the leading edge, and with experimental data by Mackowski and Williamson [9] for any pivot point location and mass distribution. For rigid foils, significant thrust enhancement due to passive heaving is found around the first natural frequency, the more so the larger the spring stiffness and the mass ratio, and when the pivot point approaches the leading edge. The first natural frequency in vacuo (23) provides a good approximation for the upper frequency limit above which no thrust amplification by passive heave can be obtained. The propulsive efficiency, however, is always smaller than that of an otherwise identical pitching-only foil without passive heave, within the present linear theory for small amplitude. Adding flexibility to the foil does not improve the propulsive performance for a given operating frequency, being the optimal frequency for flexible foils also lower than the natural frequency in vacuo (23) for given spring stiffness and mass ratio.

The results for the energy harvesting efficiency of a rigid pitching foil with passive heave are found in qualitative agreement with recent computations by Ma et al. [21], although their optimal results are not for small pitching amplitudes. It is obtained that optimal efficiency is achieved using foils with mass ratios of order ten and spring stiffness order unity or larger, pitching at, or near, the leading edge with a relatively low operating frequency. Contrary to the propulsion problem, the present results show that finite flexibility may improve substantially the energy harvesting efficiency, with an optimal stiffness ratio about four. In addition, the first natural frequency *in vacuo* (23) provides a fair estimation of the threshold frequency limit above which energy can be extracted from a given current and foil parameters.

Funding Sources

This research has been financed by the *Ministerio de Ciencia e Innovación* of Spain (PID2019-104938RB-I00) and by the Junta de Andalucía, Spain (UMA18-FEDER-JA-047 and P18-FR-1532).

A. Lift, moment and flexural coefficients

From Refs. [23, 24]:

$$C_L(t) = \pi\left[-\ddot{h} - a\ddot{\alpha} + \dot{\alpha} + A_{l2}(a)\ddot{d} + A_{l1}(a)\dot{d}\right] + C(k)\Gamma_0(t), \tag{A.1}$$

$$C_M(t) = \frac{\pi}{2}\left[a\ddot{h} + \left(a^2 + \frac{1}{8}\right)\ddot{\alpha} + \left(\frac{1}{2} - a\right)\dot{\alpha} + A_{m2}(a)\ddot{d} + A_{m1}(a)\dot{d} + A_{m0}(a)d\right] - \frac{1}{2}\left(\frac{1}{2} + a\right)C(k)\Gamma_0(t), \tag{A.2}$$

$$C_F(t) = \pi\left[-\left(a^2 + \frac{1}{4}\right)\ddot{h} - a\left(a^2 + \frac{1}{2}\right)\ddot{\alpha} + a(a-1)\dot{\alpha} + A_{f2}(a)\ddot{d} + A_{f1}(a)\dot{d} + A_{f0}(a)d\right] + \left(\frac{1}{2} + a + a^2\right)C(k)\Gamma_0(t), \tag{A.3}$$

where

$$\Gamma_0(t) = -2\pi\left[\dot{h} + \left(a - \frac{1}{2}\right)\dot{\alpha} - \alpha + A_{g1}(a)\dot{d} + A_{g0}(a)d\right] \tag{A.4}$$

is the quasi-steady circulation, with

$$C(k) = \frac{H_1^{(2)}(k)}{iH_0^{(2)}(k) + H_1^{(2)}(k)} = \mathcal{F}(k) + i\mathcal{G}(k) \tag{A.5}$$

Theodorsen's function [33], and $H_n^{(2)}(z) = J_n(z) - iY_n(z)$, $n = 0, 1$, Hankel's function of the second kind and order n, related to the Bessel functions of the first and second kind $J_n(z)$ and $Y_n(z)$ [35], and where the following functions of the pivot point location a have been defined:

$$A_{l2} = -\frac{13 + 48a^2 - 64a^3 + 24a^4}{48(1-a)^2}, \quad A_{l1} = \frac{3 + 12a - 12a^2 + 4a^3}{6(1-a)^2}, \tag{A.6}$$

$$A_{m2} = \frac{2 + 25a - 12a^2 + 52a^3 - 64a^4 + 24a^5}{48(1-a)^2}, \quad A_{m1} = \frac{-9 + 12a - 72a^2 + 56a^3 - 16a^4}{24(1-a)^2}, \tag{A.7}$$

$$A_{m0} = -\frac{3}{4(1-a)^2}, \quad A_{f2} = -\frac{35 + 32a + 392a^2 - 320a^3 + 496a^4 - 512a^5 + 192a^6}{384(1-a)^2}, \tag{A.8}$$

$$A_{f1} = \frac{1 + 8a - 18a^2 + 48a^3 - 32a^4 + 8a^5}{12(1-a)^2}, \quad A_{f0} = \frac{7 + 18a}{12(1-a)^2}, \tag{A.9}$$

$$A_{g1} = \frac{15 - 48a + 96a^2 - 80a^3 + 24a^4}{48(1-a)^2}, \quad A_{g0} = \frac{3 - 24a + 24a^2 - 8a^3}{12(1-a)^2}. \tag{A.10}$$

B. Coefficients in equation (18)

$$A_{11} = -mk^2 + k_h + b_h ik + A_{11}^F, \tag{B.1}$$

$$A_{12} = -J_a k^2 + A_{12}^F, \tag{B.2}$$

$$A_{21} = -I_a k^2 + A_{21}^F, \tag{B.3}$$

$$A_{22} = -K_d k^2 + \frac{16}{3}\frac{a^2 + \frac{1}{3}}{(1-a)^2} S + A_{22}^F, \tag{B.4}$$

$$b_1 = m(a - x_0)k^2 + b_1^F, \quad b_2 = -I_d k^2 + b_2^F, \tag{B.5}$$

where the superscript F refers to the contributions to these coefficients from the fluid-structure interaction (i.e., from C_L and C_F). Using the expressions of C_L and C_F in A, these contributions can be written as

$$A_{11}^F = \pi k[-k + 2iC(k)], \tag{B.6}$$

$$A_{12}^F = \pi \left[A_{l2}k^2 - A_{l1}ik + 2C(k)(A_{g1}ik + A_{g0})\right], \tag{B.7}$$

$$A_{21}^F = \pi \left[-\left(a^2 + \frac{1}{4}\right)k^2 + ikC(k)(2a^2 + 2a + 1)\right], \tag{B.8}$$

$$A_{22}^F = \pi \left[A_{f2}k^2 - A_{f1}ik - A_{f0} + C(k)(2a^2 + 2a + 1)\left(A_{g1}ik + A_{g0}\right)\right], \tag{B.9}$$

$$b_1^F = \pi \left\{ak^2 + ik + 2C(k)\left[1 - ik\left(a - \frac{1}{2}\right)\right]\right\}, \tag{B.10}$$

$$b_2^F = \pi \left\{\left(a^2 + \frac{1}{2}\right)ak^2 + a(a-1)ik + C(k)(2a^2 + 2a + 1)\left[1 - ik\left(a - \frac{1}{2}\right)\right]\right\}. \tag{B.11}$$

C. Functions for the time-averaged thrust coefficient

The functions $t_h(k)$, $t_{hp}(k, a, \phi)$,$t_p(k, a)$,$t_{dh}(k, a, \psi)$,$t_{pd}(k, a, \phi, \psi)$ and $t_d(k, a)$ in the time-averaged thrust coefficient (34) can be written as [24] (note that now ϕ is the phase lag of the heaving motion with respect to the prescribed pitching motion):

$$t_h = -2\mathcal{G}_1, \tag{C.1}$$

$$t_{hp} = \left[4\left(\frac{1}{4} - a\right)\mathcal{G}_1 k + \pi\left(k g_1^R - \mathcal{G}\right)\right]\cos(\phi) - \left[\pi\left(\mathcal{F} + k g_1^I\right) + \mathcal{F}_1 k + 4\mathcal{G}_1\right]\sin(\phi), \tag{C.2}$$

$$t_p = \left(\frac{1}{2} - a\right)k\left[2a\mathcal{G}_1 k + \pi\left(\mathcal{G} - k g_1^R\right)\right] - \pi\left(\mathcal{F} + k g_1^I\right) - \mathcal{F}_1 k - 2\mathcal{G}_1, \tag{C.3}$$

$$\begin{aligned} t_{hd} = &\left[\pi\left(A_{d0}^I - kA_{d1}^R - D\mathcal{G}\right) - 2A\mathcal{G}_1 k + \frac{3}{2}(E - J)\left(\pi\mathcal{G} - \frac{\mathcal{G}_1 k}{2}\right) - Q\left(\mathcal{F}_1 - \frac{\mathcal{G}_1 k}{2} + \frac{\pi\mathcal{G}}{2}\right)\right]\cos(\phi - \psi) \\ &- \left[\pi\left(-A_{d0}^R - kA_{d1}^I + D\mathcal{F}\right) - 2A\mathcal{F}_1 k + \frac{3}{2}(E - J)\left(-\frac{\mathcal{F}_1 k}{2} - \pi\mathcal{F}\right) + Q\left(\frac{\mathcal{F}_1 k}{2} + \frac{\pi\mathcal{F}}{2} + \mathcal{G}_1\right)\right]\sin(\phi - \psi), \end{aligned} \tag{C.4}$$

$$
\begin{aligned}
t_{pd} =& \left\{ \pi \left[\left(\frac{1}{2} - a \right) k \left(-A^I_{d0} + kA^R_{d1} + D\mathcal{G} \right) + A^R_{d0} + kA^I_{\mathrm{d1}} - D\mathcal{F} \right] + 2Ak \left[-a\mathcal{G}_1 k + \mathcal{F}_1 + \frac{\pi}{2} \left(kg^R_1 - \mathcal{G} \right) \right] + \right. \\
& \frac{3}{2}(E-J) \left[\pi \left(\mathcal{F} - \left(\frac{3}{4} - a \right) \mathcal{G}k + \frac{k^2}{4} g^R_1 \right) + \frac{k}{2} \left(\mathcal{F}_1 - a\mathcal{G}_1 k \right) \right] - \\
& \left. Q \left[\pi \left(\frac{k}{2}(a-1)\mathcal{G} + \mathcal{F} + \frac{kg^I_1}{2} + \frac{k^2}{4} g^R_1 \right) + \left(a + \frac{1}{2} \right) \mathcal{F}_1 k + \mathcal{G}_1 \left(1 - \frac{ak^2}{2} \right) \right] \right\} \cos(\psi) \\
& - \left\{ \pi \left[- \left(\frac{1}{2} - a \right) k \left(A^R_{d0} + kA^I_{d1} - D\mathcal{F} \right) - A^I_{d0} + kA^R_{d1} + D\mathcal{G} \right] + 2Ak \left(a\mathcal{F}_1 k + \frac{\pi}{2} \left(\mathcal{F} + kg^I_1 \right) + \mathcal{G}_1 \right) + \right. \\
& \frac{3}{2}(E-J) \left[\frac{k}{2} \left(a\mathcal{F}_1 k + \mathcal{G}_1 \right) - \pi \left(\mathcal{G} + \left(\frac{1}{4} - a \right) \mathcal{F}k - \frac{k^2}{4} g^I_1 \right) \right] - \\
& \left. Q \left[\frac{\pi}{2} k \left(a\mathcal{F} + \frac{kg^I_1}{2} - g^R_1 \right) - \mathcal{F}_1 \left(1 - \frac{ak^2}{2} \right) + \left(a + \frac{1}{2} \right) \mathcal{G}_1 k \right] \right\} \sin(\psi),
\end{aligned}
\tag{C.5}
$$

$$
\begin{aligned}
t_d =& \frac{\pi}{4} \left\{ Q \left[-kA^I_{d0} + 2A^R_{d0} + 2kA^I_{d1} + k^2 A^R_{d1} - 2A\mathcal{G}k + D(\mathcal{G}k - 2\mathcal{F}) + (E-J) \left(3\mathcal{F} - \frac{9\mathcal{G}k}{4} \right) \right] + \right. \\
& \left. k \left(4A + \frac{3E}{2} - \frac{3J}{2} \right) \left[A^I_{d0} - kA^R_{d1} + \mathcal{G} \left(-D + \frac{3E}{2} - \frac{3J}{2} \right) \right] + Q^2 \left(\frac{\mathcal{G}k}{2} - \mathcal{F} \right) \right\},
\end{aligned}
\tag{C.6}
$$

where the following functions of the pivot point location a have been used:

$$
A(a) = a^2 \left(1 + \frac{2a}{3(1-a)} + \frac{a^2}{6(1-a)^2} \right), \quad B(a) = 2a \left(1 + \frac{a}{1-a} + \frac{a^2}{3(1-a)^2} \right), \tag{C.7}
$$

$$
D(a) = 1 + \frac{2a}{1-a} + \frac{a^2}{(1-a)^2}, \quad E(a) = \frac{2}{3(1-a)} \left(1 + \frac{a}{1-a} \right), \quad J(a) = \frac{1}{6(1-a)^2}, \tag{C.8}
$$

$$
Q(a) = 2B(a) - 2D(a) + 3E(a) - 3J(a); \tag{C.9}
$$

$\mathcal{F}(k)$ and $\mathcal{G}(k)$ are the real and imaginary parts of Theodorsen's function (A.5), and likewise $\mathcal{F}_j(k)$ and $\mathcal{G}_j(k)$, $j = 1, 2, 3$, in relation to the complex functions $C_j(k)$, defined as,

$$
C_1(k) = \frac{\frac{1}{k} e^{-ik}}{iH^{(2)}_0(k) + H^{(2)}_1(k)}, \quad C_2(k) = \frac{H^{(2)}_2(k)}{iH^{(2)}_0 + H^{(2)}_1(k)}, \quad C_3(k) = \frac{Y_0(k) - iJ_2(k) + iH^{(1)}_1(k)}{iH^{(2)}_0 + H^{(2)}_1(k)}, \tag{C.10}
$$

and $g^R_j(k)$ and $g^I_j(k)$, $j = 0, 1, 2, 3, 4$, in relation to the complex functions

$$
g_0(k) = \frac{-2i}{\pi} C_1(k), \quad g_1(k) = -\frac{2}{\pi k}(1+ik)C_1(k) - \frac{i}{k} C(k), \quad g_2(k) = -\frac{1}{k} C_2(k) + \left(\frac{2i}{k^2} - \frac{2+ik}{k} \right) C_1(k), \tag{C.11}
$$

$$
g_3(k) = \frac{3Y_2(k) - kY_1(k) + iJ_3(k) - iJ_2(k)}{k^2 \left[iH^{(2)}_0 + H^{(2)}_1(k) \right]} + \frac{6}{\pi k}(1+ik) \left(\frac{2}{k^2} - 1 \right) C_1(k), \tag{C.12}
$$

$$g_4(k) = \frac{1}{iH_0^{(2)} + H_1^{(2)}(k)} \left\{ \frac{1}{k^2}\left[kJ_4(k) - 3J_3(k)\right] + \frac{ik}{4} G_{1,3}^{2,0}\left(\frac{k^2}{4} \middle| \begin{matrix} -\frac{3}{2} \\ -3, 0, -\frac{1}{2} \end{matrix} \right) \right\}$$
$$+ \frac{2}{\pi}\left[\frac{24}{k^4}(k-i) - \frac{4}{k^2}(k-3i) - i\right] C_1(k), \tag{C.13}$$

with J_ν and Y_ν the Bessel functions of the first and second kind, respectively, of order ν, and $G_{p,q}^{m,n}\left(z|\mathbf{a}_p;\mathbf{b}_q\right)$ the Meijer G-function [35]. Finally, $A_{dj}^R(k,a)$ and $A_{dj}^I(k,a)$, $j = 0, 1$, are the real and imaginary parts of the functions

$$A_{d0}(k,a) = -Bg_0 + D[1 + 2g_1(k) - C(k)] - E\left[\frac{1}{2} + 3g_2 + \frac{C}{2}\right] + J\left[4g_3 + \frac{C}{2} + \frac{C_3}{k}\right], \tag{C.14}$$

$$A_{d1}(k,a) = Ag_0 - Bg_1 + Dg_2 - E\left[g_3 - \frac{i}{2k}C\right] + J\left[g_4 - \frac{C_2}{2k}\right]. \tag{C.15}$$

References

[1] Platzer, M., Jones, K., Young, J., and Lai, J., "Flapping wing aerodynamics: progress and challenges," *AIAA J.*, Vol. 46, 2008, pp. 2136–2149. https://doi.org/10.2514/1.29263

[2] Wu, T. Y., "Fish swimming and bird/insect flight," *Ann. Rev. Fluid Mech.*, Vol. 43, 2011, pp. 25– 58. https://doi.org/10.1146/annurev-fluid-122109-160648

[3] Wu, X., Zhang, X., Tian, X., Li, X., and Lu, W., "A review on fluid dynamics of flapping foils," *Ocean Eng.*, Vol. 195, 2020, p. 106712. https://doi.org/10.1016/j.oceaneng.2019.106712

[4] Heathcote, S., and Gursul, I., "Flexible flapping airfoil propulsion at low Reynolds numbers," *AIAA J.*, Vol. 45, 2007, pp. 1066–1079. https://doi.org/10.2514/1.25431

[5] Zhu, Q., "Numerical simulation of a flapping foil with chodwise or spanwise flexibility," *AIAA J.*, Vol. 45, 2007, pp. 2448–2457. https://doi.org/10.2514/1.28565

[6] Dewey, P. A., Boschitsch, B. M., Moored, K. W., Stone, H. A., and Smits, A. J., "Scaling laws for the thrust production of flexible pitching panels," *J. Fluid Mech.*, Vol. 732, 2013, pp. 29–46. https://doi.org/10.1017/jfm.2013.384

[7] Smits, A. J., "Undulatory and oscillatory swimming," *J. Fluid Mech.*, Vol. 874, 2019, pp. P1, 1–70. https://doi.org/10.1017/jfm.2019.284

[8] Murray, M. M., and Howle, L. E., "Spring stiffness influence on an oscillating propulsor," *J. Fluids Structures*, Vol. 17, 2003, pp. 915–926. https://doi.org/10.1016/S0889-9746(03)00026-4

[9] Mackowski, A. W., and Williamson, C. H. K., "Effect of pivot point location and passive heave on propulsion from a pitching airfoil," *Phys. Rev. Fluids*, Vol. 2, 2017, p. 013101. https://doi.org/10.1103/PhysRevFluids.2.013101

[10] McKinney, W., and DeLaurier, J., "Wingmill: An oscillating-wing windmill," *AIAA J. Energy*, Vol. 5 (2), 1981, p. 109. https://doi.org/10.2514/3.62510

[11] Jones, K. D., and Platzer, M. F., "Numerical Computation of Flapping-Wing Propulsion and Power Extraction," *AIAA Paper 97-0826*, 1997. https://doi.org/10.2514/6.1997-826

[12] Peng, Z., and Zhu, Q., "Energy harvesting through flow-induced oscillations on a foil," *Phys. Fluids*, Vol. 21, 2009, p. 123602. https://doi.org/10.1063/1.3275852

[13] Young, J., Lai, J. C. S., and Platzer, M. F., "A review of progress and challenges in flapping foil power generation," *Prog. Aero. Sci.*, Vol. 67, 2014, pp. 2–28. https://doi.org/10.1016/j.paerosci.2013.11.001

[14] Xiao, Q., and Zhu, Q., "A review on flow energy harvesting based on flapping foils," *J. Fluids Structures*, Vol. 46, 2014, pp. 174–191. https://doi.org/10.1016/j.jfluidstructs.2014.01.002

[15] Veilleux, J. C., and Dumas, G., "Numerical optimization of a fully-passive flapping-airfoil turbine," *J. Fluids Structures*, Vol. 70, 2017, pp. 102–130. https://doi.org/10.1016/j.jfluidstructs.2017.01.019

[16] Zhu, Y., Su, Y., and Breuer, K., "Nonlinear flow-induced instability of an elastically mounted pitching wing," *J. Fluid Mech.*, Vol. 899, 2020, p. A35. https://doi.org/10.1017/jfm.2020.481

[17] Zhu, Q., and Peng, Z., "Mode coupling and flow energy harvesting by a flapping foil," *Phys. Fluids*, Vol. 21, 2009, p. 033601. https://doi.org/10.1063/1.3092484

[18] Liu, W., Xiao, Q., and Cheng, F., "A bio-inspired study on tidal energy extraction with flexible flapping wings," *Bioinspir. Biomim.*, Vol. 8, 2013, p. 036011. https://doi.org/10.1088/1748-3182/8/3/036011

[19] Deng, J., Teng, L., Pan, D., and Shao, X., "Inertial effects of the semi-passive flapping foil on its energy extraction efficiency," *Phys. Fluids*, Vol. 27, 2015, p. 053103. https://doi.org/10.1063/1.4921384

[20] Su, Y., and Breuer, K., "Resonant response and optimal energy harvesting of an elastically mounted pitching and heaving hydrofoil," *Phys. Rev. Fluids*, Vol. 4, 2019, p. 064701. https://doi.org/10.1103/PhysRevFluids.4.064701

[21] Ma, P., Liu, G., Wang, Y., Zhang, Y., and Xie, Y., "Numerical study on the hydrodynamic performance of a semi-passive oscillating hydrofoil," *Ocean Eng.*, Vol. 223, 2021, p. 108649. https://doi.org/10.1016/j.oceaneng.2021.108649

[22] Alaminos-Quesada, J., and Fernandez-Feria, R., "Propulsion of a foil undergoing a flapping undulatory motion from the impulse theory in the linear potential limit," *J. Fluid Mech.*, Vol. 883, 2020, pp. A19, 1–24. https://doi.org/10.1017/jfm.2019.870

[23] Fernandez-Feria, R., and Alaminos-Quesada, J., "Analytical results for the propulsion performance of a flexible foil with prescribed pitching and heaving motions and passive small deflection," *J. Fluid Mech.*, Vol. 910, 2021, p. A43. https://doi.org/10.1017/jfm.2020.1015

[24] Fernandez-Feria, R., and Alaminos-Quesada, J., "Propulsion and energy harvesting performances of a flexible thin airfoil undergoing forced heaving motion with passive pitching and deformation of small amplitude," *J. Fluids Structures*, Vol. 102, 2021, p. 103255. https://doi.org/10.1016/j.jfluidstructs.2021.103255

[25] Alben, S., "Optimal flexibility of a flapping appendage in an inviscid fluid," *J. Fluid Mech.*, Vol. 614, 2008, pp. 355–380. https://doi.org/10.1017/S0022112008003297

[26] Moore, M. N. J., "A fast Chebyshev method for simulating flexible-wing propulsion," *J. Comput. Phys.*, Vol. 345, 2017, pp. 792–817. https://doi.org/10.1016/j.jcp.2017.05.052

[27] Floryan, D., and Rowley, C. W., "Clarifying the relationship between efficiency and resonance for flexible inertial swimmers," *J. Fluid Mech.*, Vol. 853, 2018, pp. 271–300. https://doi.org/10.1017/jfm.2018.581

[28] Michelin, S., and Llewellyn Smith, S. G., "An unsteady point vortex method for coupled fluid-solid problems," *Theor. Comput. Fluid Dyn.*, Vol. 23, 2009, pp. 127–153. https://doi.org/10.1007/s00162-009-0096-7

[29] Alben, S., Witt, C., Baker, T. V., Anderson, E., and Lauder, G. V., "Dynamics of freely swimming flexible foils," *Phys. Fluids*, Vol. 24, 2012, p. 051901. https://doi.org/10.1063/1.4709477

[30] Moore, M. N. J., "Torsional spring is the optimal flexibility arrangement for thrust production of a flapping wing," *Phys. Fluids*, Vol. 27, 2015, p. 091701. https://doi.org/10.1063/1.4930235

[31] Paraz, F., Schouvelier, L., and Eloy, C., "Thrust generation by a heaving foil: Resonance, nonlinearities, and optimality," *Phys. Fluids*, Vol. 28, 2016, p. 011903. https://doi.org/10.1063/1.4939499

[32] Moore, M. N. J., "Analytical results on the role of flexibility in flapping propulsion," *J. Fluid Mech.*, Vol. 757, 2014, pp. 599–612. https://doi.org/10.1017/jfm.2014.533

[33] Theodorsen, T., "General theory of aerodynamic instability and the mechanism of flutter," Tech. Rep. TR 496, NACA, 1935.

[34] Garrick, I. E., "Propulsion of a flapping and oscillating airfoil," Tech. Rep. TR 567, NACA, 1936.

[35] Olver, F. W. J., Lozier, D. W., Boisvert, R. F., and Clark, C. W. (eds.), *NIST handbook of mathematical functions*, Cambridge University Press, Cambridge (UK), 2010.